

Water uptake and energetics of formation of barium zirconate based multicomponent oxides

Aleksandra Mielewczyk-Gryń¹, Tamilarasan Subramani², Daniel Jaworski¹, Kristina Lilova², Wojciech Skubida¹, Alexandra Navrotsky², and Maria Gazda¹

¹Institute of Nanotechnology and Materials Engineering, Faculty of Applied Physics and Mathematics, and Advanced Materials Centre, Gdańsk University of Technology, Narutowicza 11/12 80-233 Gdańsk, Poland

²School of Molecular Sciences and Center for Materials of the Universe, Arizona State University, Tempe, AZ 85287, USA

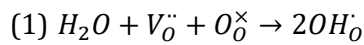
Abstract

A group of multi-component oxides based on BaZrO₃ has been prepared using the solid-state reaction method and examined in terms of water uptake and thermodynamics of formation. Depending on the type and amount of acceptor substitution, the synthesized compounds exhibit various proton defect concentrations, reaching up to 0.2 mol/mol for a compound containing 10 different elements in the B-sublattice, where 50% of them are acceptors. For the most promising materials, the van't Hoff plots were done and the enthalpies and entropies of hydration were calculated. At higher temperatures, these parameters do not differ from values for reference yttrium doped barium zirconate. However, at lower temperatures they are more negative, indicating a more exothermic process of proton incorporation.

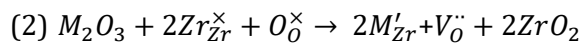
Introduction

Current state-of-the-art materials for protonic ceramic electrochemical cells (PCECs) are developed to maximize performance.¹⁻³ One way to enhance performance is by using multicomponent oxides as electrodes and electrolytes.² This enables tuning properties like electronic and ionic conductivities to meet the strict requirements for long-term efficient operation. Especially in the field of electrolytes, the modification of the barium cerate-zirconate system is widely investigated and materials such as BaCe_{0.7}Zr_{0.1}Y_{0.1}Yb_{0.1}O₃ are currently applied in operating devices.² In theory, incorporating a higher number of constituent oxides, which serve as acceptors, will enhance the material's performance by elevating the number of oxygen

vacancies in the case of ion conductors and by producing more sites available for the hydration reaction (1).



The electroneutrality reaction for acceptor doping in barium zirconate can be described as (2), where M is a trivalent cation, usually Y or Yb. However, the maximum reported dopant concentration in barium zirconate is in the range of 20-50 mol %, thus limiting the number of vacancies.⁴⁻⁸ Moreover, the conductivity of this system is limited by the effect of vacancy clustering which limits the protonic conductivity at a certain level for material with dopant content exceeding 20 mol %.



One of the ways of introducing a higher concentration of dopants is to enhance the stability of the material by introducing a higher variety of constituent oxides. This is why high entropy/multi constituent oxides have been developed in recent years.⁹ The interest in this group of materials stemmed from the research on high entropy alloys. These designed multi-component alloys were named "high-entropy alloys" (HEAs) by Yeh et al. which suggests the high configurational entropy of the random mixing of elements in these alloys.¹⁰ Similarly, the approaches to producing configurational entropy stabilized multiconstituent oxides have been stated in 2015 by Rost et al. in their work on MgO, NiO, ZnO, CuO, and CoO-based oxides.¹¹ Our previous work went a step further and facilitated the multiplicity of cations in one of the sublattices to alter electrical properties.¹² We studied a series of multiconstituent oxides based on barium zirconate and showed that they exhibit protonic conductivity. In the current work, we present data on the energetics of the formation of various multicomponent oxides based on barium zirconate. Moreover, we investigated the thermodynamics of the hydration of materials with substantial water uptake. For the first time, such a study has been undertaken for multiconstituent proton conductors.

Experimental Methods

The compositions of the samples and the abbreviations used for naming them are shown in Table 1. All samples were produced by conventional solid-state synthesis. Stoichiometric amounts of BaCO₃, ZrO₂, HfO₂, SnO₂, TiO₂, CeO₂, Y₂O₃, Yb₂O₃, In₂O₃, Sm₂O₃, and ZnO powders (all of > 99.9% purity) were initially mixed using an agate mortar and then ball-milled in isopropanol for 24 h (Fritsch Pulverisette 7). The rotation speed was set at 600 rpm, and the ball-to-powder ratio was 3:1. After drying at 80 °C for 24 h, the powder samples were calcined at 950 °C for 24 h with a heating/cooling rate of 5 °C/min in ambient atmosphere. Samples were then reground in isopropanol with 1 wt % polyvinyl butyral (PVB), dried, and sieved through a 100 μm sieve. The obtained powders were pressed into rectangular pellets using uniaxial pressure of 350 MPa for 2 min. Sample pellets except for BZHST_Ce_Y_In_Sm_Yb_Zn were annealed at 1500 °C for 10 h with a heating rate of 5 °C/min and cooling in the furnace. The BZHST_Ce_Y_In_Sm_Yb_Zn sample was annealed at 1150 °C. The samples have been crushed into bulk powder with a surface area below 5 m²/g. To check the influence of water on crystal structure, the specimen with the highest proton concentration was hydrated in the tube furnace with a flux of wet air ($p_{H_2O} = 0.021$ atm, $p_{O_2} = 0.21$ atm) at 300 °C for 24 h.

Table 1 Samples' naming used in this work

No.	Composition	Sample ID
1	BaZr _{0.2} Hf _{0.2} Sn _{0.2} Ti _{0.2} Ce _{0.2} O ₃	BZHST_Ce
2	BaZr _{0.2} Hf _{0.2} Sn _{0.2} Ti _{0.2} Y _{0.2} O _{2.9}	BZHST_Y
3	BaZr _{0.2} Hf _{0.2} Sn _{0.2} Ti _{0.2} Sm _{0.2} O _{2.9}	BZHST_Sm
4	BaZr _{0.2} Hf _{0.2} Sn _{0.2} Ti _{0.2} In _{0.2} O _{2.9}	BZHST_In
5	BaZr _{0.2} Hf _{0.2} Sn _{0.2} Ti _{0.2} Yb _{0.2} O _{2.9}	BZHST_Yb
6	BaZr _{0.125} Hf _{0.125} Sn _{0.125} Ti _{0.125} Y _{0.125} In _{0.125} Sm _{0.125} Yb _{0.125} O _{2.75}	BZHST_Y_In_Sm_Yb
7	BaZr _{0.1} Hf _{0.1} Sn _{0.1} Ti _{0.1} Ce _{0.1} Y _{0.1} Sm _{0.1} In _{0.1} Zn _{0.1} Yb _{0.1} O _{2.7}	BZHST_Ce_Y_In_Sm_Yb_Zn

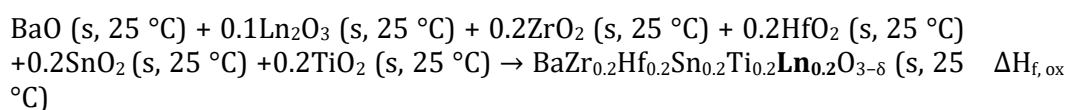
The samples were analyzed by powder X-ray diffraction (XRD) using a Philips X'Pert PRO diffractometer operated with Cu K α radiation at room temperature. The analysis of the diffraction patterns and Rietveld refinements were conducted with the HighScore Plus software. As the starting point for the refinement, the BaZrO₃ structural data were used (COD 1538369). To derive strain and crystallite size information during Rietveld refinement structural parameters obtained

from LaB_6 were used as a standard (NIST SRM 660a). High-temperature oxide melt solution calorimetry, on pre-dried samples, was carried out using a Setaram AlexSYS Tian-Calvet twin microcalorimeter by methods standard to our laboratory and described previously.¹³ The calorimeter was calibrated against the heat content of high-purity $\alpha\text{-Al}_2\text{O}_3$ (99.99%). Pressed sample pellets (~5 mg) were dropped from ambient temperature into the calorimeter containing the solvent, molten sodium molybdate ($3\text{Na}_2\text{O}\cdot 4\text{MoO}_3$), in a silica glass crucible at 800 °C. All experiments used oxygen bubbling through the solvent at 5 mL/min to aid dissolution and prevent local saturation of the solvent.

An example of the thermodynamic cycle used in calculating formation enthalpies from oxides ($\Delta H_{f, \text{ox}}$) at 25 °C is shown in Table 2. The drop solution calorimetry values used in these calculations are presented in Table 3. One could reason that in the case of such complicated stoichiometries like those studied here the information about the stability relative to ternary oxides could be an issue. Nevertheless, thermodynamic stability relative to binary oxides allows us to determine the general trends in stability. Moreover, some end members as perovskite oxides are believed to be unstable concerning their binary oxides due to the large difference between constituent cations ionic radii, therefore, we are not able to synthesize the given perovskite end-members.

Table 2 Thermodynamic cycle used for calculations of formation enthalpies at room temperature

Reaction	ΔH (kJ mol ⁻¹)
$\text{BaZr}_{0.2}\text{Hf}_{0.2}\text{Sn}_{0.2}\text{Ti}_{0.2}\text{Ln}_{0.2}\text{O}_{3-\delta}$ (s, 25 °C) \rightarrow BaO (dis, 800 °C) + 0.1Ln ₂ O ₃ (dis, 800 °C) + 0.2ZrO ₂ (dis, 800 °C) + 0.2HfO ₂ (dis, 800 °C) + 0.2SnO ₂ (dis, 800 °C) + 0.2TiO ₂ (dis, 800 °C)	$\Delta H_1 = \Delta H_{\text{ds}} \dagger$
BaO (s, 25 °C) \rightarrow BaO (dis, 800 °C)	ΔH_2
Ln ₂ O ₃ (s, 25 °C) \rightarrow Ln ₂ O ₃ (dis, 800 °C)	ΔH_3
ZrO ₂ (s, 25 °C) \rightarrow ZrO ₂ (dis, 800 °C)	ΔH_4
HfO ₂ (s, 25 °C) \rightarrow HfO ₂ (dis, 800 °C)	ΔH_5
SnO ₂ (s, 25 °C) \rightarrow SnO ₂ (dis, 800 °C)	ΔH_6
TiO ₂ (s, 25 °C) \rightarrow TiO ₂ (dis, 800 °C)	ΔH_7



$$\Delta H_{f, \text{ox}} = -\Delta H_1 + \Delta H_2 + 0.1\Delta H_3 + 0.2\Delta H_4 + 0.2\Delta H_5 + 0.2\Delta H_6 + 0.2\Delta H_7$$

†For BZHST_Ce following formula was used for the calculation: $\text{BaZr}_{0.2}\text{Hf}_{0.2}\text{Sn}_{0.2}\text{Ti}_{0.2}\text{Ce}_{0.2}\text{O}_3 \text{ (s, 25 °C)} \rightarrow \text{BaO (dis, 800 °C)} + 0.2\text{CeO}_2 \text{ (dis, 800 °C)} + 0.2\text{ZrO}_2 \text{ (dis, 800 °C)} + 0.2\text{HfO}_2 \text{ (dis, 800 °C)} + 0.2\text{SnO}_2 \text{ (dis, 800 °C)} + 0.2\text{TiO}_2 \text{ (dis, 800 °C)}$

Table 3 Enthalpies of drop solution (ΔH_{ds}) in sodium molybdate solvent at 800°C used for calculations

Oxide	ΔH_{ds} (kJ mol ⁻¹)
BaO	-176.48 ± 3.48 ¹⁴
ZrO ₂	29.20 ± 1.2 ¹⁵
TiO ₂	73.74 ± 0.48 ¹⁶
SnO ₂	52.85 ± 0.21 ¹⁷
HfO ₂	23.90 ± 1.1
In ₂ O ₃	12.23 ± 1.03 ¹⁷
ZnO	20.68 ± 0.7 ¹⁸
Y ₂ O ₃	-116.34 ± 1.21 ¹⁹
CeO ₂	76.78 ± 0.75 ^{20,21*}
Sm ₂ O ₃	-131.99 ± 1.6 ¹⁹
Yb ₂ O ₃	-82.65 ± 1.06 ²²

*Recalculated from 700°C including heat content difference

Thermogravimetric analysis of water uptake was performed using a Netzsch Jupiter 449 F1 (Netzsch GmbH, Selb, Germany). Approximately 2.5 g of as-prepared powder was placed in a 5 mL alumina crucible, heated to 800 °C, and held at this temperature for 5 h under dry air to remove water and any surface carbon dioxide. To determine the differences between hydration levels for multiple compositions, an isothermal switch between dry and humidified gas at 300 °C was performed. The purge gas (synthetic air or nitrogen) was then saturated with water ($p_{\text{H}_2\text{O}} = 0.021$ atm). Additionally, for samples with substantial water uptake BZHST_Y_In_Sm_Yb and BZHST_Ce_Y_In_Sm_Yb_Zn), the weight change was recorded upon cooling to determine the thermodynamics of hydration. Data were collected every 50 °C in the temperature range 800 – 300 °C with a 3 h stabilization time at each temperature. The procedure has been previously successful and validated for the determination of hydration energetics in barium zirconates.²³



Results and Discussion

Hydration energetics

X-ray diffraction patterns for all samples have been indexed within the barium zirconate cubic structure (Pm-3m space group) (Figure 1S and 2S). Refinement quality and structural data derived from Rietveld refinements for all synthesized samples are presented in Table 1S. No additional phases were identified, indicating a complete reaction and no phase separation of the compounds during the synthesis. The effect of hydration on the crystal structure of BZHST_Ce_Y_In_Sm_Yb_Zn is depicted in Figures 3S and 4S. Incorporated water expands the unit cell, changing the lattice parameter from 4.2564(1) Å to 4.2831(1) Å. Therefore, this shows that water uptake takes place in studied materials.

Table 4 Water uptake at 300 °C for all studied compositions.

Sample ID	Nominal acceptor concentration (mol%)	$[OH_O^\bullet]$ in air (mol/mol)	$[OH_O^\bullet]$ in N ₂ (mol/mol)
BZHST_Ce	0	$2.1 \cdot 10^{-3}$	$2.1 \cdot 10^{-3}$
BZHST_Y	20	$3.6 \cdot 10^{-2}$	$3.7 \cdot 10^{-2}$
BZHST_Sm	20	$2.5 \cdot 10^{-2}$	$2.9 \cdot 10^{-2}$
BZHST_In	20	$3.7 \cdot 10^{-2}$	$4.0 \cdot 10^{-2}$
BZHST_Yb	20	$3.0 \cdot 10^{-2}$	$3.5 \cdot 10^{-2}$
BZHST_Y_In_Sm_Yb	50	$1.5 \cdot 10^{-1}$	$1.5 \cdot 10^{-1}$
BZHST_Ce_Y_In_Sm_Yb_Zn	60	$2.0 \cdot 10^{-1}$	$2.1 \cdot 10^{-1}$

Table 4 summarizes the obtained values of water uptake. For all studied compositions, the values obtained in air and nitrogen atmosphere are similar. This suggests that the availability of sites for hydration is the same in both oxidizing and inert atmospheres. Moreover, the highest value of water uptake was found for samples with 8 and 10 cations in the B sublattice –**having the highest number of acceptors**, in air 0.15 mol/mol for BZHST_Y_In_Sm_Yb and 0.2 mol/mol for BZHST_Ce_Y_In_Sm_Yb_Zn. The values obtained for these two compositions are of the same order of magnitude as the one reported for barium zirconate and barium cerate.^{6,23,24,25} Thus, these two compounds have been chosen to study hydration thermodynamics. The sample weight changes with temperature under dry and wet atmospheres for BZHST_Y_In_Sm_Yb and BZHST_Ce_Y_In_Sm_Yb_Zn, both in N₂ and air, are presented in Figure 6S. The shape of the hydration curves is **like** those reported for barium zirconate by Goncalves et al. and Yamazaki et

al. and is typical of protonic conductors.^{6,23} Figure 1 presents the proton concentration of investigated samples at different temperatures as well as equilibrium constant K_{hydr} versus reciprocal temperature. The proton concentration gradually decreases with increasing temperature and is very similar for both studied compounds. The $\log K_{hydr}(1/T)$ plot shows linear behavior in two distinctive temperature ranges (above and below 500 °C). Based on these relations the enthalpy and entropy of hydration have been determined. Proton incorporation for this system can be summarized as reaction (1), where the equilibrium constant of this reaction is represented as equation (3). The values of equilibrium constant are based on the nominal dopant concentration ($[OH_O^\bullet] + 2[V_O^{\bullet\bullet}] = [A']$) assuming that the hole concentration under the measurement condition is negligible ($p \approx 0$). Consequently, the equilibrium constant can be projected using equation (4), where: [O] oxygen site concentration; [A'] acceptor (nominal) concentration.

$$(3) K_{hydr} = \frac{[OH_O^\bullet]^2}{[V_O^{\bullet\bullet}][O_O^\times]p_{H_2O}} = \exp\left(\frac{\Delta S_{hydr}}{R}\right) \exp\left(-\frac{\Delta H_{hydr}}{RT}\right)$$

$$(4) K_{hydr}^{p=0} = \frac{4}{p_{H_2O}} \frac{[OH_O^\bullet]^2}{([O] - [OH_O^\bullet])^2 - ([O] - [A'])^2} \quad \text{where } [O] = [O_O^\times] + [V_O^{\bullet\bullet}] + [OH_O^\bullet] \text{ is oxygen sites concentration}$$

The calculation of the energetics of hydration was done separately for two temperature ranges (see Figure 1 and Table 5).

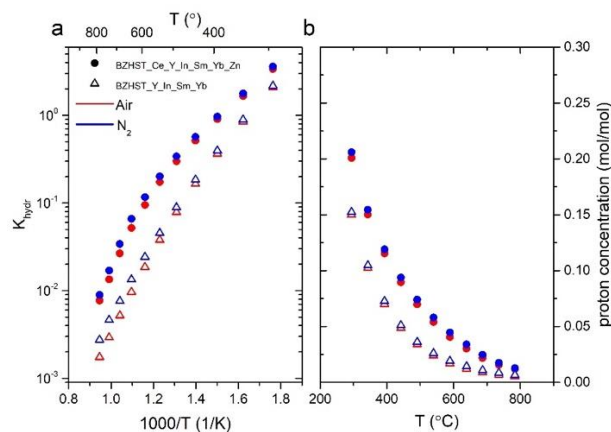


Figure 1 a) Equilibrium constant for water incorporation reaction calculated for both studied compositions using eq. (4). b) Temperature dependence of proton defect concentration.

The data for the barium zirconate system (Table 5) have been added for comparison. The values for BZHST_Y_In_Sm_Yb and BZHST_Ce_Y_In_Sm_Yb_Zn are similar and comparable to the ones obtained by us previously for the barium zirconate system.²³ This shows similar energetics of hydration for all the studied materials. Putilov and Tsidilkovski suggested that the trapping-related components of thermodynamic functions can be divided into contributions of protons and vacancies. Trapping of protons makes the hydration reaction more exothermic and decreases the hydration entropy.²⁶ On the other hand, trapping of oxygen vacancies makes hydration less favorable due to the higher stability of bound vacancies. Simultaneously, the filling of oxygen vacancies due to hydration leads to a decrease in the entropy linked to a more ordered distribution of vacancies over bound and free positions.

The hydration enthalpy, entropy, and Gibbs free energy for yttrium doped barium zirconate-cerate have an unusual non-monotonic dependence on dopant content.²⁶ Therefore the dependence on composition for multiconstituent oxides can be even more complex. However, the comparison of hydration energetics gives no direct indication that the introduction of multiple cations within the same sublattice enhances proton trapping. Therefore, it is potentially possible to introduce a higher amount of dopants than for barium zirconate without decreasing proton mobility due to trapping.

Moreover, Bjørheim et al.'s calculations of the relations between the chemical expansion of oxygen vacancies and hydration thermodynamics in barium zirconate show that the hydration entropy primarily originates from the entropy change upon filling the oxygen vacancy, which is closely related to the chemical expansion coefficient of oxygen vacancies, and thus the chemical expansion upon hydration.²⁷ Additionally, they suggest that problems related to chemical expansion upon hydration of BaZrO₃ to some extent can be avoided, or reduced, by partial substitution of Zr by Ce. Therefore, it can be assumed that the introduction of multiple cations in the zirconium sublattice can influence this parameter as well.

Table 5 Hydration energetics of studied compositions

Material	Atm.	Temperature range (°C)	p _{H2O} (atm)	Hydr. Enthalpy, (kJ mol ⁻¹)	Hydr. entropy (J mol ⁻¹ K ⁻¹)	Source	
BZHST_Y_In_Sm_Yb	air	800 – 550	0.019	-90 ± 1	-138 ± 1	This work	
		500 – 300		-60 ± 2	-99 ± 3		
	N ₂	800 – 550		-82 ± 2	-126 ± 2		
		500 – 300		-58 ± 2	-96 ± 3		
BZHST_Ce_Y_In_Sm_Yb_Zn	air	800 – 550	0.019	-92 ± 4	-127 ± 5	This work	
		500 – 300		-44 ± 1	-67 ± 1		
	N ₂	800 – 550		-92 ± 6	-124 ± 6		
		500 – 300		-43 ± 1	-65 ± 1		
BaZr _{0.9} Y _{0.1} O _{2.95}	air	900 – 500	0.019	-94 ± 12	-131 ± 13	23	
		500 – 100		-18 ± 2	-35 ± 3		
BaZr _{0.8} Y _{0.2} O _{2.9}	air	900 – 500	0.019	-98 ± 12	-122 ± 13	23	
		500 – 200		-22 ± 4	-25 ± 6		
	N ₂	500 – 50		0.023	-22 ± 1	-39 ± 1	28
		900 – 550		0.023	-93.3	-103.2	25
BaZr _{0.7} Y _{0.3} O _{2.85}	air	900 – 500	0.019	-141 ± 20	-166 ± 20	23	
		500 – 300		-25 ± 6	-28 ± 9		
BaZr _{0.6} Y _{0.4} O _{2.8}	N ₂	500 – 50	0.023	-26 ± 1	-41 ± 1	28	
BaZr _{0.5} Ce _{0.4} Y _{0.1} O _{3-δ}	N ₂	1200 – 600	0.019	-41.64	-46.89	29	
BaZr _{0.44} Ce _{0.35} Y _{0.2} O _{3-δ}	N ₂	1200 – 600		-42.72	-47.15		

Energetics of formation

To evaluate how the introduction of multiple cations influences the thermodynamic stability of the initial dry phases, oxide melt solution calorimetry has been undertaken to obtain the enthalpies of formation at room temperature. Figure 2 presents the enthalpy of formation from oxides of anhydrous/dried samples at room temperature versus configurational entropy calculated in a single lattice model ($S_{config}^{single\ lattice} = -R \sum_i X_i \ln X_i$)^{9,30} and the entropy metrics (EM) stemming from configurational entropy in the sublattice model. Here we use the entropy metrics defined as (5) with S_{config}^{SL} defined as (6), where a_{SL} is the number of sites on the s sublattice, and X_i is the fraction of element species randomly distributed on the s sub-lattice or the site fraction proposed by Diplo and Vecchio.³⁰ By this metric, it is possible not only to account for the number of atoms in a particular sublattice but also the number of sublattices.

$$EM = \frac{S_{config}^{SL}}{R} \cdot L \quad (5)$$

$$S_{config}^{SL} = \frac{-R \sum_{SL} \sum_i a_{SL} [X_i] \ln[X_i]}{\sum_{SL} a_{SL}} \quad (6)$$

Table 6 Values of enthalpy of drop solution and of formation from oxides at room temperature of studied oxides for pre-dried materials. Uncertainties calculated as two standard deviations of the mean.

Sample ID	ΔH_{ds} (kJ/mol)	$\Delta H_{f,ox}$ (kJ/mol)
BZHST_Ce	-25.72 ± 1.07	-99.47 ± 6.71
BZHST_Y	-51.43 ± 0.89	-100.75 ± 6.51
BZHST_Sm	-39.49 ± 0.61	-114.25 ± 6.31
BZHST_In	-36.56 ± 0.55	-102.76 ± 6.27
BZHST_Yb	-46.75 ± 0.43	-102.06 ± 6.27
BZHST_Y_In_Sm_Yb	-111.37 ± 1.20	-62.57 ± 6.81
BZHST_Ce_Y_In_Sm_Yb_Zn	-106.04 ± 0.89	-58.66 ± 6.49

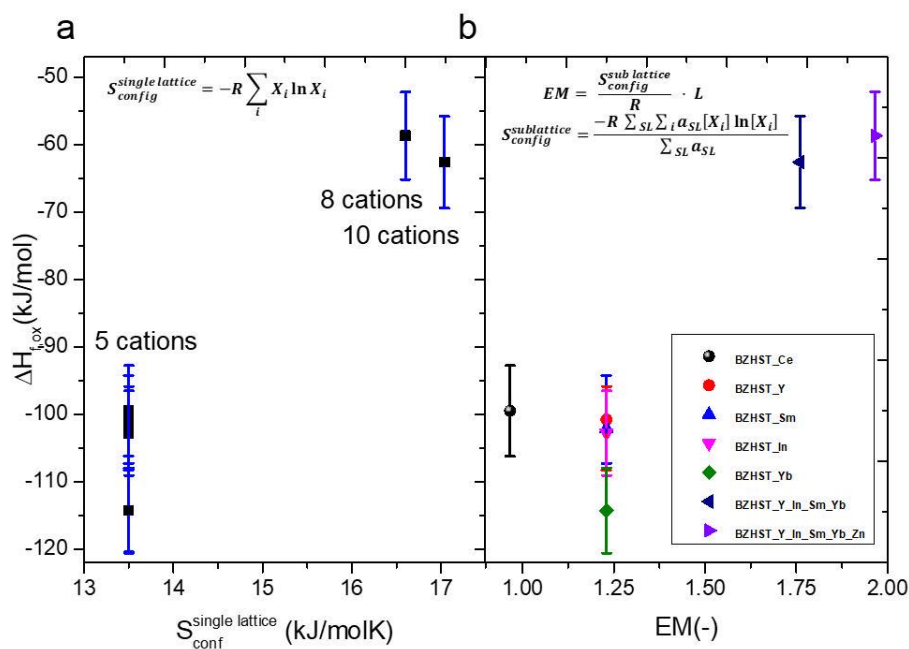


Figure 2 Enthalpies of drop solution formation from the oxides at 25 °C as a function of configurational entropy for a single lattice model ($S_{conf}^{single\ lattice}$) and entropy metrics (EM) based on the sublattice model ($S_{conf}^{sublattice}$). The experimental uncertainties are indicated.

Dippo and Vecchio's entropy metrics consider the number of *sites* on the sublattice, and the fraction of element species (cation or anion) distributed on the sublattice. This method can be applied to compare different crystalline materials, including solid solutions as well as high entropy materials with complex crystal structures and multiple sublattices. This model is similar to the one proposed by McCormack and Navrotsky⁹, except the configurational entropy is J/(K*mol per atom) instead of J/(K*mol per formula unit) as the number of sites in the crystal structure is included.³¹ With this approach, it is easier to compare the materials with the same number of constituents but with different chemical states. In our case, this model was used to differentiate between BZHSTCe and samples with lanthanides with a 3+ oxidation state. For both approaches to calculation/assessment of configurational entropy illustrated in Figure 3, two groups of materials can be differentiated: one with 5 cations which have more exothermic enthalpies of formation from oxides, and one with 8 and 10 cations. Table 6 summarizes the values of enthalpies of formation from oxides and drop solution enthalpies for all studied compositions.

According to Dippo and Vecchio, materials with EM > 1.5 should be considered as high entropy, while between 1 and 1.5 as medium entropy oxides. Figure 2 shows that samples that can be assigned to a group with high entropy exhibit far less exothermic enthalpies of formation from oxides than the ones with lower EM/configurational entropy.

The materials with EM < 1.5 have similar and more exothermic enthalpies of formation. The maximum value of configurational enthalpy means the maximization of random configurations of atoms within the structure. However, in multicomponent oxide systems, the ideal mixing assumption is often violated due to short-, mid-, and long-range ordering of cations and/or anions.⁹ Therefore, [the assumption of "high entropy" can be therefore altered by this, and the free energy of formation can be different from that calculated assuming random mixing.](#) This aspect



can be especially important in a view of multiple works describing “high-entropy oxides” without any in-depth thermodynamic analysis.³² Deviations from randomness leading to clustering of like atoms generally make the enthalpy of formation less exothermic. Deviations leading to order make it more exothermic. Both types of deviations diminish the configurational entropy. Because of this complexity, one needs to study the effects of clustering and ordering on different length scales on the thermodynamics of a given system carefully to effectively design new HEOs, especially new ionic conductors. One can compare the current values with the one obtained by Goncalves et al. for yttrium-doped barium zirconate $\text{BaZr}_{1-x}\text{Y}_x\text{O}_3$. In their study, the enthalpy of formation for doping range $x = 0$ to 0.5 becomes less negative when increasing yttrium content from undoped (-115.12 ± 3.69 kJ/mol) to $x = 0.5$ (-77.09 ± 4.31 kJ/mol). The comparison between multi-constituent BZHST_Y sample with nominal 20% yttrium in the zirconium sublattice and $\text{BaZr}_{0.8}\text{Y}_{0.2}\text{O}_3$ exhibit $\Delta H_{f,ox}$ equal to $-100,75 \pm 6.51$ kJ/mol and -92.84 ± 3.87 kJ/mol respectively. This shows that the introduction of multiple cations into the zirconium sublattice does not influence the energetics of formation significantly. This is extremely important because of the possibility of the introduction of high concentrations of dopants without compromising stability, thus allowing the tunability of properties of the barium zirconate system. By using high concentrations of particular dopants, we will be able to tune both ionic and electronic contributions to conductivity. Therefore, we will be able not only to address issues with electrolytes but also electrodes for operating devices. Moreover, the values for high-entropy materials, BZHST_Y_In_Sm_Yb (total of 0.875 mole content of other cations in Zr sublattice) and BZHST_Ce_Y_In_Sm_Yb_Zn (total of 0.9 other cations), being -62.57 ± 6.81 kJ/mol and -58.66 ± 6.49 kJ/mol, are in the same range as that for $\text{BaZr}_{0.5}\text{Y}_{0.3}\text{O}_3$ (-78.82 ± 3.88 kJ/mol). It has been reported for barium zirconate that for higher yttrium substitution the perovskite structure is destabilized due to lattice distortions and the formation of oxygen vacancies.⁴ We do not observe this in the case of the studied compositions. Tsvetkov et al. reported the enthalpy of formation from oxides for barium cerate to be -51.65 kJ/mol while Matschkevich reported -36.2 ± 3.4 kJ/mol for indium doped barium cerate.^{33,34} The enthalpies of formation for all studied compositions show

that the energetics of the formation of barium zirconate-based multi-constituent oxides have similar values to those for the base BaZrO_3 composition. The introduction of multiple cations on one of the sublattices does not significantly change the energetics in comparison to the classic low entropy perovskite even for a high concentration of acceptor substituents.

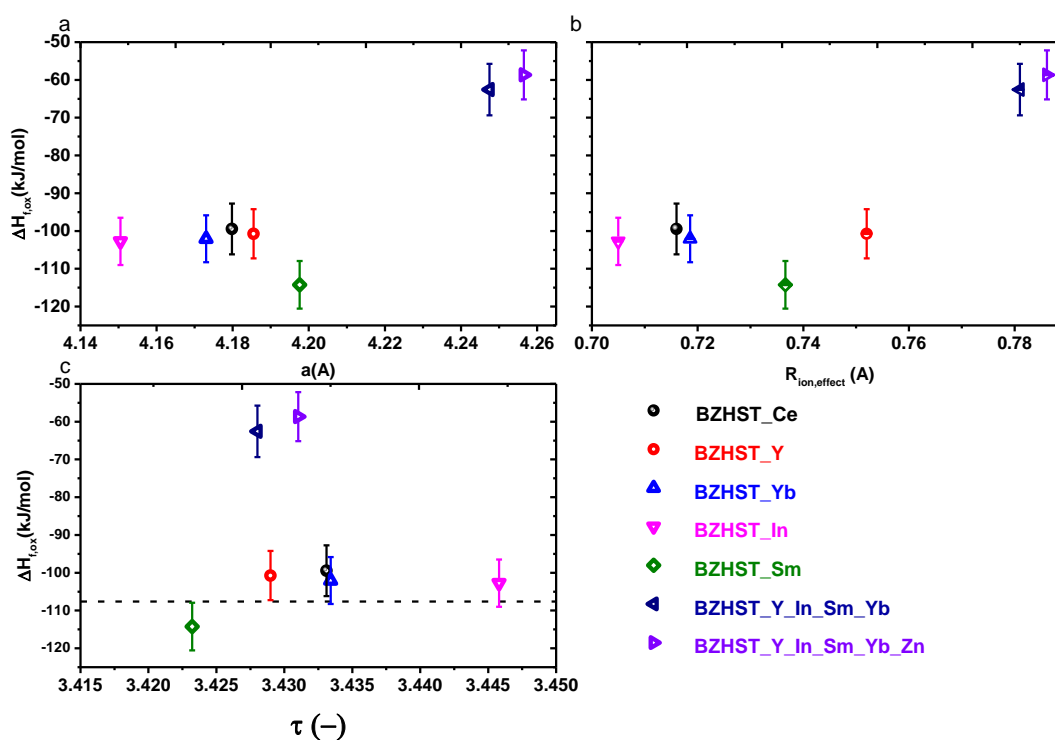


Figure 3 Enthalpies of drop solution formation from the oxides at 25 °C as a function of unit cell parameter (a), average ionic radius of B-cation (b), and extended Goldschmidt factor³⁵ (c), ionic radii according to Shannon.³⁶ The experimental uncertainties are indicated.

Figures 3 a) and b) depict the [relationship](#) between the enthalpy of formation from oxides and the unit cell parameter of the cubic structure computed from Rietveld refinement and average ionic radii on the B site, respectively. The unit cell parameters are the highest for the samples with the largest number of cations. For these samples, we also observe less negative enthalpies of formation. The highest value of average B-site ionic radii is correlated with less exothermic $\Delta H_{f,ox}$. This is contrary to the general trend observed for low entropy perovskites in which the larger ionic radii correspond to higher thermodynamic stability. Figure 3c shows the relation of enthalpy

of formation and extended structural factor

$$\tau = \frac{r_x}{r_B} - n_A \left(n_A - \frac{r_A/r_B}{\ln(r_A/r_B)} \right)$$
 where n_A is the oxidation state of A, r_i is the ionic radius of ion i, $r_A > r_B$

by definition, and $\tau < 4.18$ indicates stable perovskite.³⁵ All studied samples have calculated τ values lower than 3.5. For compositions with similar τ and the same number of cations, the enthalpies of formation are similar. For samples with a higher number of cations, namely BZHST_Y_In_Sm_Yb and BZHST_Y_In_Sm_Yb_Zn, the thermodynamic stability decreases (enthalpy of formation from oxides become less exothermic). This all shows that the introduction of the **chemical complexity** does not lead to the **significantly** lower stability of the perovskite structure given the enthalpy of formation from oxides, **which are for all studied compositions strongly exothermic**. The introduction of multiple cations on the zirconium sublattice does not decrease the stability significantly in comparison to yttrium-doped barium zirconate, which gives high hopes to tuning the system properties without paying a thermodynamic price.

Conclusion

Multicomponent oxides based on barium zirconate have been successfully synthesized by the solid-state synthesis route. The energetics of formation and hydration have been measured by calorimetry. The formation energetics of the materials with low and medium entropy metrics follow the same trend as undoped and low doped barium zirconate, while the compositions with high entropy metrics share similar values as highly doped yttrium doped barium zirconate. The hydration energetics of samples with high entropy metrics show hydration enthalpies like those for acceptor-doped barium zirconates and cerates. Their water uptake is also in the same range as barium zirconate. This all shows that it is possible to introduce high amounts of other constituents to the zirconium sublattice to potentially change various properties without paying a significant price in thermodynamic stability.

Acknowledgments

The research was financially supported by the National Science Centre (NCN), Poland, within the project 2019/35/B/ST5/00888. AM-G acknowledges financial support from the Gdańsk

University of Technology by the DEC-2/2020/IDUB/IV.2/EUROPIUM grant under the European Short-Term Outgoing Visits - 'Excellence Initiative - Research University'. The calorimetry at Arizona State University was supported by financial support from the U.S. Department of Energy, Office of Basic Energy Sciences, Grant DE-SC0021987.

References

- 1 D. Medvedev, Trends in research and development of protonic ceramic electrolysis cells, *Int J Hydrogen Energy*, 2019, **44**, 26711–26740.
- 2 C. Duan, J. Huang, N. Sullivan and R. O'Hayre, Proton-conducting oxides for energy conversion and storage, *Appl Phys Rev*, 2020, **7**, 011314.
- 3 J. Kim, S. Sengodan, S. Kim, O. Kwon, Y. Bu and G. Kim, Proton conducting oxides: A review of materials and applications for renewable energy conversion and storage, *Renew Sustain Energy Rev*, 2019, **109**, 606–618.
- 4 M. D. Gonçalves, P. S. Maram, R. Muccillo and A. Navrotsky, Enthalpy of formation and thermodynamic insights into yttrium doped BaZrO₃, *J Mater Chem A Mater*, 2014, **2**, 17840–17847.
- 5 M. D. Gonçalves and R. Muccillo, Properties of yttrium-doped barium zirconate ceramics synthesized by the oxidant-peroxo method, *Ceram Int*, 2014, **40**, 911–917.
- 6 Y. Yamazaki, P. Babilo and S. M. Haile, Defect chemistry of yttrium-doped barium zirconate: A thermodynamic analysis of water uptake, *Chem Mater*, 2008, **20**, 6352–6357.
- 7 Y. Yamazaki, R. Hernandez-Sanchez and S. M. Haile, Cation non-stoichiometry in yttrium-doped barium zirconate: phase behavior, microstructure, and proton conductivity, *J Mater Chem*, 2010, **20**, 8158.
- 8 F. Giannici, A. Longo, A. Balerna, K. Kreuer and A. Martorana, Proton Dynamics in BaZrO₃ : Insights on the Atomic and Electronic Structure from X-ray Absorption Spectroscopy, *Chem Mater*, 2009, **21**, 2641–2649.
- 9 S. J. McCormack and A. Navrotsky, Thermodynamics of high entropy oxides, *Acta Mater*, 2021, **202**, 1–21.
- 10 Y. Jien-Wei, S.-K. Chen, S.-J. Lin, J.-Y. Gan, T.-S. Chin, T.-T. Shun, C.-H. Tsau and S.-Y. Chang, Nanostructured High-Entropy Alloys with Multiple Principal Elements: Novel Alloy Design Concepts and Outcomes, *Adv Eng Mater*, 2004, **6**, 299–304.
- 11 C. M. Rost, E. Sacht, T. Borman, A. Moballeggh, E. C. Dickey, D. Hou, J. L. Jones, S. Curtarolo and J. P. Maria, Entropy-stabilized oxides, *Nat Commun*, 2015, **6**, 8485.
- 12 M. Gazda, T. Miruszewski, D. Jaworski, A. Mielewczyk-Gryń, W. Skubida, S. Wachowski, P. Winiarz, K. Dzierzgowski, M. Łapiński, I. Szpunar and E. Dzik, Novel Class of Proton Conducting Materials - High Entropy Oxides, *ACS Mater Lett*, 2020, **2**, 1315-1321.

- 13 A. Navrotsky, Progress and New Directions in Calorimetry: A 2014 Perspective, *J Am Ceram Soc*, 2014, **97**, 3349–3359.
- 14 W. Gong and A. Navrotsky, Thermodynamics of BaNd₂O₄ and phase diagram of the BaO-Nd₂O₃ system, *J Mater Res*, 2019, **34**, 3337–3342.
- 15 D. L. Drey, E. C. O’Quinn, T. Subramani, K. Lilova, G. Baldinozzi, I. M. Gussev, A. F. Fuentes, J. C. Neufeind, M. Everett, D. Sprouster, A. Navrotsky, R. C. Ewing and M. Lang, Disorder in Ho₂Ti_{2-x}Zr_xO₇: pyrochlore to defect fluorite solid solution series, *RSC Adv*, 2020, **10**, 34632-34650.
- 16 S. Hayun and A. Navrotsky, Formation enthalpies and heat capacities of rear earth titanates: RE₂TiO₅ (RE=La, Nd and Gd), *J Solid State Chem*, 2012, **187**, 70–74.
- 17 M. Abramchuk, K. Lilova, T. Subramani, R. Yoo and A. Navrotsky, Corrigendum to: Development of high-temperature oxide melt solution calorimetry for p-block element containing materials (*J Mater Res*, 2020, 35, 16, (2239-2246), 10.1557/jmr.2020.185), *J Mater Res*, 2021, **36**, 785.
- 18 T. Subramani, K. I. Lilova, M. Householder, S. Yang, J. Lyons and A. Navrotsky, Surface energetics of wurtzite and sphalerite polymorphs of zinc sulfide and implications for their formation in nature, *Geochim Cosmochim Acta*, 2023, **340**, 99–107.
- 19 A. Mielewczyk-Gryn and A. Navrotsky, Enthalpies of formation of rare earth niobates, RE₃NbO₇, *Am Mineral*, 2015, **100**, 1578–1583.
- 20 A. Navrotsky, W. Lee, A. Mielewczyk-Gryn, S. V. Ushakov, A. Anderko, H. Wu and R. E. Riman, Thermodynamics of solid phases containing rare earth oxides, *J Chem Thermodyn*, 2015, **88**, 126–141.
- 21 R. Robie and B. S. Hemingway, Thermodynamic Properties of Minerals and Related Substances at 298.15K and 1 Bar, *U.S. Geological Survey Bulletin*, 1995, 1–461.
- 22 J. Qi, X. Guo, A. Mielewczyk-Gryn and A. Navrotsky, Formation enthalpies of LaLnO₃ (Ln=Ho, Er, Tm and Yb) interlanthanide perovskites, *J Solid State Chem*, 2015, **227**, 150–154.
- 23 M. D. Gonçalves, A. Mielewczyk-Gryn, P. S. Maram, Ł. Kryścio, M. Gazda and A. Navrotsky, Systematic Water Uptake Energetics of Yttrium Doped Barium Zirconate - A High Resolution Thermochemical Study, *J Phys Chem C*, 2020, **124**, 11308–11316
- 24 T. Schober, H.G. Bohn, Water vapor solubility and electrochemical characterization of the high temperature proton conductor BaZr_{0.9}Y_{0.1}O_{2.95}, *Solid State Ion*, 2000, **127**, 351-360
- 25 K. D. Kreuer, St. Adams, W. Münch, A. Fuchs, U. Klock and J. Maier, Proton conducting alkaline earth zirconates and titanates for high drain electrochemical applications, *Solid State Ion*, 2001, **145**, 295–306.
- 26 L. P. Putilov and V. I. Tsidilkovski, Impact of bound ionic defects on the hydration of acceptor-doped proton-conducting perovskites, *Phys Chem Chem Phys*, 2019, **21**, 6391–6406.
- 27 T. S. Bjørheim, A. Løken and R. Haugsrud, On the relationship between chemical expansion and hydration thermodynamics of proton conducting perovskites, *J Mater Chem A Mater*, 2016, **4**, 5917-5924.
- 28 Y. Yamazaki, C.-K. K. Yang and S. M. Haile, Unraveling the defect chemistry and proton uptake of yttrium-doped barium zirconate, *Scr Mater*, 2011, **65**, 102–107.



- 29 K. Leonard, Y. S. Lee, Y. Okuyama, K. Miyazaki and H. Matsumoto, Influence of dopant levels on the hydration properties of SZCY and BZCY proton conducting ceramics for hydrogen production, *Int J Hydrogen Energy*, 2017, **42**, 3926–3937.
- 30 O. F. Dippo and K. S. Vecchio, A universal configurational entropy metric for high-entropy materials, *Scr Mater*, 2021, **201**, 113974.
- 31 Y. Sharma, M. C. Lee, K. C. Pitike, K. K. Mishra, Q. Zheng, X. Gao, B. L. Musico, A. R. Mazza, R. S. Katiyar, V. Keppens, M. Brahlek, D. A. Yarotski, R. P. Prasankumar, A. Chen, V. R. Cooper and T. Z. Ward, High Entropy Oxide Relaxor Ferroelectrics, *ACS Appl Mater Interfaces*, 2022, **14**, 11962–11970.
- 32 M. Brahlek, M. Gazda, V. Keppens, A. R. Mazza, S. J. McCormack, A. Mielewczyk-Gryń, B. Musico, K. Page, C. M. Rost, S. B. Sinnott, C. Toher, T. Z. Ward and A. Yamamoto, What is in a name: Defining "high entropy" oxides, *APL Mater*, 2022, **10**, 110902.
- 33 N. I. Matskevich, Enthalpy of formation of $\text{BaCe}_{0.9}\text{In}_{0.1}\text{O}_{3-\delta}$, *J Therm Anal Calorim*, 2007, **90**, 955–958.
- 34 D. S. Tsvetkov, V. V. Sereda, D. A. Malyshkin, A. L. Sednev-Lugovets, A. Y. Zuev and I. L. Ivanov, Thermodynamics of formation of solid solutions between BaZrO_3 and BaPrO_3 , *Chim Techno Acta*, 2021, **7**, 42–50.
- 35 C. J. Bartel, C. Sutton, B. R. Goldsmith, R. Ouyang, C. B. Musgrave, L. M. Ghiringhelli and M. Scheffler, New tolerance factor to predict the stability of perovskite oxides and halides, *Sci Adv*, 2019, **5**, 1–10.
- 36 R. D. Shannon, Revised effective ionic radii and systematic studies of interatomic distances in halides and chalcogenides, *Acta Crystallogr A*, 1976, **32**, 751–767.